Biomechanics and Modeling in Mechanobiology (2021) 20:861–878
https://doi.org/10.1007/s10237-020-01407-3

ORIGINAL PAPER

Electro-magnetically modulated self-propulsion of swimming sperms via cervical canal

Sara I. Abdelsalam[1,2] · Jorge X. Velasco-Hernández[1] · A. Z. Zaher[3]

Received: 11 October 2020 / Accepted: 26 November 2020 / Published online: 31 March 2021

Abstract
The purpose of this study is to theoretically investigate the electro-magneto-biomechanics of the swimming of sperms through cervical canal in the female reproductive system. During sexual intercourse, millions of sperms migrate into the cervix in large groups, hence we can approximately model their movement activity by a swimming sheet through the electrically-conducting biofluid. The Eyring–Powell fluid model is considered as the base fluid to simulate male's semen with self-propulsive sperms. An external magnetic field is applied on the flow in transverse direction. The governing partial differential system of equations is analytically solved. Creeping flow regimen is employed throughout the channel due to self-propulsion of swimmers along with long wavelength approximation. Solutions for the stream function, velocity profile, and pressure gradient (above and below the swimming sheet) are obtained and plotted with the pertinent parameters. The prominent features of pumping characteristics are also investigated. Results indicate that the propulsive velocity is reduced with an increase in the electric field which is an important feature that can be used in controlling the transport of spermatozoa inside the cervical canal. Not only is the present analysis valid for living micro-organisms, but also valid for artificially designed electro-magnetic micro-swimmers which is further utilized in electro-magnetic therapy taking place in female's lubricous cervical canal filled with mucus.

Keywords Electro-magnetic therapy · Eyring–Powell fluid · Swimming sperms transport · Mucus velocity · Propulsive velocity · Cervical flow

1 Introduction

The study of sperm transmission has widely been studied by many researchers (Taylor 1951; Reynolds 1965; Tuck 1968; Pak and Lauga 2010; Shack and Lardner 1974; Davajan et al. 1970; Odeblad 1962; Smelser et al. 1974; Shukla et al. 1978, 1988; Sinha et al. 1982; Philip and Chandra 1995; Radhakrishnamacharya and Sharma 2007; Walait et al. 2018). These researchers focused on understanding the state-of-the-art behind the traveling of the spermatozoa in the vagina through the body fluids that fills the cervical waterway. Passage of sperms through the cervix (the transmission of sperm within the uterine canal) is considered an important study because it helps conserve the health of sperms that in turn affects the human reproduction and maintains the existence of life. Generally, most of the sperms get lost at some point at the vaginal level by ejecting some sperms from the vaginal opening and the rest of sperms which could make it through the vagina are the ones that are studied by researchers. One mechanism of sperm transportation was proposed by Davajan et al. (1970) and explained by Odeblad (1962). The latter ones attempted to elucidate the rapid rate of sperm transition with efficacy between the mucus and the swimming sperm. The long-chained molecules of high molecular weight, that are of a complicated suspension, in an exceedingly lower molecular weight fluid is named by cervical mucus. The cervix commonly acts as an obstacle

✉ Sara I. Abdelsalam
sara.abdelsalam@bue.edu.eg; siabdelsalam@im.unam.mx; siabdelsalam@yahoo.com

A. Z. Zaher
abdullah.zaher@feng.bu.edu.eg

1 Instituto de Matemáticas - Juriquilla, Universidad Nacional Autónoma de México, Blvd. Juriquilla 3001, 76230 Querétaro, Mexico

2 Basic Science, Faculty of Engineering, The British University in Egypt, Al-Shorouk City, Cairo 11837, Egypt

3 Engineering Mathematics and Physics Department, Faculty of Engineering, Shubra-Benha University, Cairo, Egypt

that hinders the transport of sperms but with the secretion of suitable amounts of cervical mucus, the transport of sperms through the vagina is being facilitated. Cervical mucus is secreted by tissue cells (non-ciliated epithelial cells) that line the cervical canal. Smelser et al. (1974) provided an explanation for the sperm transport via the cervical mucus based totally on the dynamic interplay between the cervical mucus and the swimming of sperms that was recommended by Davajan et al. (1970). Also, Walait et al. (2018) simulated the cervix as a 2D channel with waves propagating on the flexible slippery walls of the cervix. They discovered that the chance of the spermatozoa to fertilize an ovum is maximized when the slippage on the upper cervical wall is maximum along with zero slippage on the lower wall of the cervix. An additional assumption that has been going around is that a spermatozoon takes a form of an infinite pliable sheet which drives itself in the opposite direction to traveling waves of the cervical mucus by the flow of the propulsive waves. Asghar et al. (2019) presented the dynamic of the sperm, as a swimming micro-organism, under the effect magnetic field where they took the cervical mucus fluid as Carreau fluid model. They found that the magnetic force in the negative direction is an assistive force to the motion of sperm.

The combination of magnetic fields with propulsive flows has important applications in biomedical engineering problems (Bhatti et al. 2020; Eldesoky et al. 2019; Abd Elmaboud et al. 2019; Sohail et al. 2020a, 2020d; Abdelsalam and Bhatti 2018; Abdelsalam and Vafai 2017; Zhang et al. 2020; Mekheimer et al. 2013). The magnetohydrodynamic flow of sperms' motility through the cervix is important in relation with certain flow problems involving conductive physiological fluids. It helps integrate the sperms with mucus liquid, and it helps in the treatment of chronic medical conditions, such as vaginal stenosis, using the magnetic vaginal dilator (Morris et al. 2017). It has considerable nonmechanical micro-pumping properties that has remarkable applications especially if accompanied with electric field (electro-magnetohydrodynamic flows, known as "EMHD"), some of which, flow control in microfluidic systems, fluid pumping, and fluid blending (Morris et al. 2017; Mekheimer et al. 2017; Keramati et al. 2016; Buren and Jian 2015; Bhatti et al. 2017; Abo-Elkhair et al. 2018; Ellahi et al. 2020; Dharmendra et al. 2020; Zeeshan et al. 2019). Lorentz force is produced as a result of two fields; one of these fields is the electric field force which is carried out throughout the channel in the presence of the magnetic field force. The combination between these two fields is called the electromagnetic forces. Contrasted with different kinds of nonmechanical micro-pumps, the EMHD micro-pumps can be employed in many aspects such as in regular flow control and bidirectional siphoning potential.

One of the most important models for non-Newtonian fluids is the Eyring–Powell fluid model since it can be deduced from the kinetic theory of liquids rather than from the empirical relation. It can also be reduced to the Newtonian behavior for low and high shear rates. Ishaq et al. (2019) studied the 2D nanofluid for the Eyring–Powell fluid model with magnetic field on a permeable stretching sheet. They concluded that the magnetic field has a decreasing effect on the velocity distribution of nanofluid. Oyelami and Dada (2016) investigated the magnetohydrodynamics of an Eyring–Powell fluid model with viscous dissipation and thermal radiation effects where they found out that the flow decelerates with an increase in the non-Newtonian parameter. Ellahi et al. (2016) investigated the slip, and heat transfer effects on the Eyring–Powell fluid in the presence of a magnetic field. They deduced that the Hartmann number has a quite opposite impact on the velocity distribution than that of the slip parameter. Khan et al. (2017) studied the anisotropic slip, and magnetic field effects on an Eyring–Powell fluid with heat transfer over a rotating disk where they discovered that the slip-length boundary condition has a great impact on the temperature and velocity profiles.

During copulation, seminal fluid is being deposited inside the vagina (by either seminal emission at high arousal levels or propulsatile ejaculation), and those which are not being ejected outside the vagina are the ones that can approach the cervix. The action of this sperm motility requires a special PH level which is being buffered by the upper vagina and last for only few minutes providing enough time for the sperms' motility (Nakano et al. 2015). Such rapid motion of sperms along with the muscular peristaltic movement of the female's reproductive tract cannot, however, guarantee the capability of swimming through the cervical mucus and fertilizing an egg successfully (Carlson 2019). Several factors must be taken place for fertility and pregnancy to occur such as having healthy sperms. A healthy spermatozoon has a rounded head with long and strong tail. Other factors which are taken into account are assuming that the man is healthy, non-obese, non-smoker, and does not have low sperms count (not under 10 million sperms per ml) so that it does not affect fertility and assuming also there no cervical constriction or stenosis in the female's reproductive system (Nakano et al. 2015; Jones and Lopez 2014; Durairajanayagam 2018; Kay et al. 2013; Sohail et al. 2020b, 2020c; Abdelsalam and Sohail 2020; Naz et al. 2019).

With the above taken factors and limitations into consideration, we intend to study the electro-magnetohydrodynamics of swimming sperms through cervical canal using Eyring–Powell fluid model as the base fluid. The EMHD is expected to have novel consequences along with the pressure difference that is expected to affect the probability of pregnancy. The current research gives a simple theoretical estimate of the interactivity of swimming sperms with the walls in the vicinity and may aid in the electro-magnetic therapy and/or electrovaginogram (Shafik et al. 2004). Multiple factors are investigated in this model such as the propulsive velocity, Eyring–Powell fluid parameter, Hartmann number, wave amplitude on the cervical wall, and electric field on the physical variables of interest.

2 Electromagnetohydrodynamic non-Newtonian propulsion model

Consider a 2D cervical canal of a female's reproductive system constituting micro-organisms (swimming sperms) with speed V_p taking place from the vagina to the uterus in a negative X-direction. The transport of sperms takes place by self-propulsion in a form of a flexible sheet which pushes itself against traveling sinusoidal waves on the canal walls that propagate from the uterus to the vagina along the positive X-axis. Electromagnetic flow of Eyring–Powell fluid is used to model the transient flow. The flow is triggered by a Lorentz force $\vec{j} \times \vec{B}$ generated by two fields, namely magnetic field $\vec{B}\left(0, -B_0, 0\right)$ and electric field $\vec{E}(0, 0, E)$, where the current density is denoted by $\overrightarrow{j^{\pm}} = \sigma^* \left(\vec{E} + \overrightarrow{q^{\pm}} \times \vec{B}\right)$, and the velocity is denoted by $\vec{q}\left(\bar{U}, \bar{V}\right)$. We refer to the upper swimming sheet by a positive sign and to the lower one by a negative sign. The Cartesian coordinates are used such that the X-axis is chosen along the canal, and Y-axis is normal to it. We consider that propagating waves traveling along the walls of the cervical canal have a speed c and wavelength λ. We also assume that the self-propulsive swimming sheet of sperms propagates

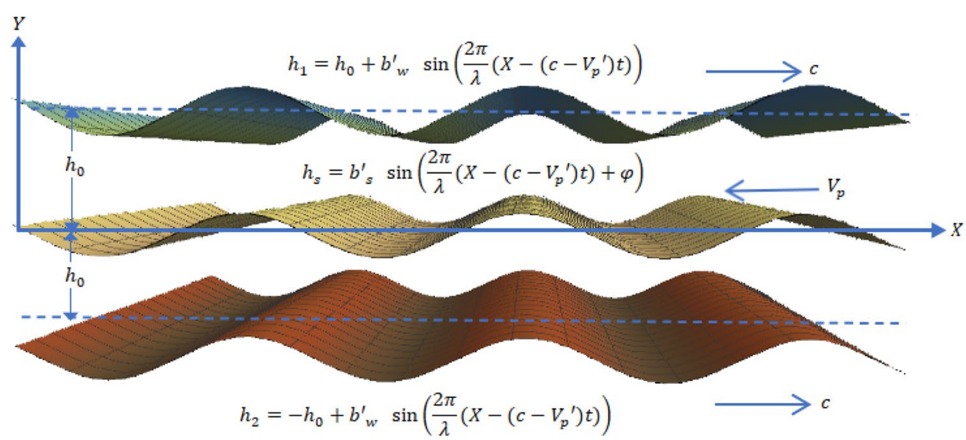

Fig. 1 Schematic diagram for the self-propulsion of swimming sheet of sperms through female's cervical canal

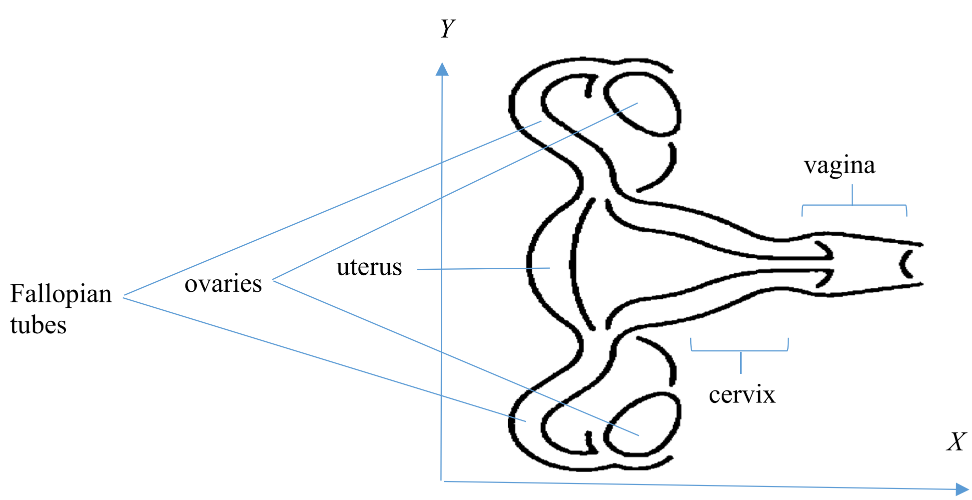

Fig. 2 Schematic diagram for the anatomy of the female reproductive system

synchronously with the moving frame of reference. The surface profiles along the walls of the cervical canal and the swimming sperms' sheet in the fixed frame, as shown in Figs. 1 and 2, are described as

$$\begin{aligned}
&\text{Upper wall} && h_1 = h_0 + b'_w \sin\left(\tfrac{2\pi}{\lambda}\left(X - \left(c - V_p{}'\right)t\right)\right)\\
&\text{Surface of swimming sperm} && h_s = b'_s \sin\left(\tfrac{2\pi}{\lambda}\left(X - \left(c - V_p{}'\right)t\right) + \varphi\right)\\
&\text{Lower wall} && h_2 = -h_0 + b'_w \sin\left(\tfrac{2\pi}{\lambda}\left(X - \left(c - V_p{}'\right)t\right)\right)
\end{aligned} \tag{2.1}$$

where the mean distance of the swimming sperm to another cervical wall (lower or upper) is represented by h_0, φ is the phase difference, and b'_s and b'_w are the amplitudes of the wave on the micro-organism swimmer surface and cervical walls, respectively.

3 Cervical fluid equations

The governing equations of motion along with the continuity equation for the 2D flow of the incompressible cervical fluid, neglecting the thermal effects, are given by

$$\rho\left(\frac{\partial \overrightarrow{q^{\pm}}}{\partial t} + \left(\overrightarrow{q^{\pm}}\cdot\nabla\right)\overrightarrow{q^{\pm}}\right) = -\nabla p^{\pm} + \nabla\cdot\tau^{\pm} + \overrightarrow{j^{\pm}}\times\vec{B}, \tag{3.1}$$

where the constitutive equation for the Eyring–Powell fluid is defined as (Ellahi et al. 2020; Dharmendra et al. 2020)

$$\tau_{ij}{}^{\pm} = \mu\frac{\partial q_i{}^{\pm}}{\partial x_j} + \frac{1}{B}\sinh^{-1}\left\{\frac{1}{C^*}\frac{\partial q_i{}^{\pm}}{\partial x_j}\right\}, \tag{3.2}$$

such that μ is the dynamic viscosity and B and C^* are the material constants of Eyring–Powell fluid. For the stress components, the function is approximated as

$$\sinh^{-1}\left\{\frac{1}{C^*}\frac{\partial q_i{}^{\pm}}{\partial x_j}\right\} = \frac{1}{C^*}\frac{\partial q_i{}^{\pm}}{\partial x_j} + \left(\frac{1}{6C^*}\frac{\partial q_i{}^{\pm}}{\partial x_j}\right)^3, \tag{3.3}$$

Then the governing equations in the two-dimensional flow are given by

$$\begin{aligned}
&\frac{\partial U^{\pm}}{\partial X} + \frac{\partial V^{\pm}}{\partial Y} = 0,\\
&\rho\left(\frac{\partial U^{\pm}}{\partial t} + U^{\pm}\frac{\partial U^{\pm}}{\partial X} + V^{\pm}\frac{\partial U^{\pm}}{\partial Y}\right)\\
&\quad = -\frac{\partial p^{\pm}}{\partial X} + \frac{\partial \tau^{\pm}_{XX}}{\partial X} + \frac{\partial \tau^{\pm}_{XY}}{\partial Y} + \sigma E B_0 + \sigma B_0^2 U^{\pm},\\
&\rho\left(\frac{\partial V^{\pm}}{\partial t} + U^{\pm}\frac{\partial V^{\pm}}{\partial X} + V^{\pm}\frac{\partial V^{\pm}}{\partial Y}\right)\\
&\quad = -\frac{\partial p^{\pm}}{\partial Y} + \frac{\partial \tau^{\pm}_{YX}}{\partial X} + \frac{\partial \tau^{\pm}_{YY}}{\partial Y},
\end{aligned} \tag{3.4}$$

The fixed and moving (laboratory) frames are related as follows

$$\begin{aligned}
&\tilde{x} = X - \left(c - V_p{}'\right)t, \quad \tilde{y} = Y,\\
&\tilde{u}^{\pm} = U^{\pm} - \left(c - V_p{}'\right),\ \tilde{v}^{\pm} = V^{\pm}.
\end{aligned} \tag{3.5}$$

In light of Eq. (3.5), the governing Eq. (3.4) of the cervical fluid become

$$\begin{aligned}
&\frac{\partial \tilde{u}^{\pm}}{\partial x} + \frac{\partial \tilde{v}^{\pm}}{\partial y} = 0,\\
&\rho\left(\tilde{u}^{\pm}\frac{\partial \tilde{u}^{\pm}}{\partial \tilde{x}} + \tilde{v}^{\pm}\frac{\partial \tilde{u}^{\pm}}{\partial \tilde{y}}\right) = -\frac{\partial \tilde{p}^{\pm}}{\partial \tilde{x}} + \frac{\partial \tau^{\pm}_{\tilde{x}\tilde{x}}}{\partial \tilde{x}}\\
&\quad + \frac{\partial \tau^{\pm}_{\tilde{x}\tilde{y}}}{\partial \tilde{y}} + \sigma E B_0 + \sigma B_0^2\left(\tilde{u}^{\pm} - V_p{}' + c\right),\\
&\rho\left(\tilde{u}^{\pm}\frac{\partial \tilde{v}^{\pm}}{\partial \tilde{x}} + \tilde{v}^{\pm}\frac{\partial \tilde{v}^{\pm}}{\partial \tilde{y}}\right) = -\frac{\partial \tilde{p}^{\pm}}{\partial \tilde{y}} + \frac{\partial \tau^{\pm}_{\tilde{y}\tilde{x}}}{\partial \tilde{x}} + \frac{\partial \tau^{\pm}_{\tilde{y}\tilde{y}}}{\partial \tilde{y}},
\end{aligned} \tag{3.6}$$

We introduce the following dimensionless parameters:

$$\begin{aligned}
&\tilde{x} = \frac{x}{\lambda},\ \tilde{y} = \frac{y}{h_0},\ \tilde{u}^{\pm} = \frac{u^{\pm}}{c},\ \tilde{v}^{\pm} = \frac{v^{\pm}}{\delta c},\\
&\tilde{p}^{\pm} = \frac{h_0^2}{\lambda\mu c^2},\ \delta = \frac{h_0}{\lambda},\ b_s = \frac{b'_s}{h_0},\\
&b_w = \frac{b'_w}{h_0} \quad \text{and} \quad V_p{}' = \frac{V_p}{c}
\end{aligned} \tag{3.7}$$

Using the dimensionless parameters in Eq. (3.7) along with the definition of the Eyring–Powell fluid in Eq. (3.2), the dimensionless equations for the fluid model can be written as

$$\begin{aligned}
&R_e\delta\left(u^{\pm}\frac{\partial u^{\pm}}{\partial x} + v^{\pm}\frac{\partial u^{\pm}}{\partial y}\right) = -\frac{\partial p^{\pm}}{\partial x}\\
&\quad + \delta^2(1+\alpha)\frac{\partial^2 u^{\pm}}{\partial x^2} - \Lambda\delta^4\left(\frac{\partial u^{\pm}}{\partial x}\right)^2\frac{\partial^2 u^{\pm}}{\partial x^2}\\
&\quad + (1+\alpha)\frac{\partial^2 u^{\pm}}{\partial y^2} - \Lambda\left(\frac{\partial u^{\pm}}{\partial u}\right)^2\frac{\partial^2 u^{\pm}}{\partial y^2}\\
&\quad + SHa - Ha^2\left(u^{\pm} - V_p + 1\right),
\end{aligned}$$

$$\begin{aligned}
&R_e\delta^3\left(u^{\pm}\frac{\partial v^{\pm}}{\partial x} + v^{\pm}\frac{\partial v^{\pm}}{\partial y}\right) = -\frac{\partial p^{\pm}}{\partial y}\\
&\quad + \delta^4(1+\alpha)\frac{\partial^2 v^{\pm}}{\partial x^2} - \Lambda\delta^8\left(\frac{\partial v^{\pm}}{\partial x}\right)^2\frac{\partial^2 v^{\pm}}{\partial x^2}\\
&\quad + \delta^2(1+\alpha)\frac{\partial^2 v^{\pm}}{\partial y^2} - \Lambda\delta^4\left(\frac{\partial v^{\pm}}{\partial u}\right)^2\frac{\partial^2 v^{\pm}}{\partial y^2},
\end{aligned} \tag{3.8}$$

where $R_e\left(=\frac{\rho c h_0}{\mu}\right)$ is Reynolds number, $\alpha\left(=\frac{1}{\mu B C^*}\right)$ and $\Lambda\left(=\frac{\alpha c^2}{2h_0^2 C^{*2}}\right)$ are Eyring–Powell fluid parameters, $S\left(=\frac{h_0 E_s}{c}\sqrt{\frac{\sigma}{\mu}}\right)$ is the electric field strength, and $Ha\left(=h_0 B_0\sqrt{\frac{\sigma}{\mu}}\right)$ is Hartmann number. Using the approximation $\delta = \frac{2\pi h_0}{\lambda} \ll 1$ and $\frac{1}{C^*} \ll 1$, i.e. $\Lambda \ll 1$. Then Eq. (3.8) becomes

$$0 = -\frac{\partial p^{\pm}}{\partial x} + (1+\alpha)\frac{\partial^2 u^{\pm}}{\partial y^2} + SHa - Ha^2\left(u^{\pm} - V_p + 1\right), \qquad 0 = -\frac{\partial p^{\pm}}{\partial y}, \tag{3.9}$$

with corresponding boundary conditions

$$u^{\pm} = V_p - 1 \text{ at } y = h_{1,2}, \qquad u^{\pm} = -1 \text{ at } y = h_s. \tag{3.10}$$

where $h_1 = 1 + b_w \sin(2\pi x)$, $h_2 = -1 + b_w \sin(2\pi x)$, and $h_s = b_s \sin(2\pi(x+\varphi))$.

Using the boundary conditions (3.10), the solution of Eq. (3.9) takes the form:

Cervical upper fluid

$$u^{+}(y) = \frac{1}{Ha^2}\left(-\frac{\partial p^{+}}{\partial x} + Ha(S + Ha(-1+V_p)) + \mathrm{Csch}\left(\frac{(h_1-h_s)Ha}{\sqrt{1+\alpha}}\right)\left(\left(\frac{\partial p^{+}}{\partial x} - Ha(S+HaV_p)\right)\mathrm{Sinh}\left(\frac{Ha(h_1-y)}{\sqrt{1+\alpha}}\right) + \left(-\frac{\partial p^{+}}{\partial x} + HaS\right)\mathrm{Sinh}\left(\frac{Ha(h_1-y)}{\sqrt{1+\alpha}}\right)\right)\right), \tag{3.11}$$

Cervical lower fluid

$$u^{-}(y) = \frac{1}{Ha^2}\left(-\frac{\partial p^{-}}{\partial x} + Ha\left(S + Ha\left(-1+V_p\right)\right) + \mathrm{Csch}\left(\frac{\left(h_2-h_s\right)Ha}{\sqrt{1+\alpha}}\right)\left(\left(\frac{\partial p^{-}}{\partial x} - Ha\left(S+HaV_p\right)\right)\mathrm{Sinh}\left(\frac{Ha\left(h_2-y\right)}{\sqrt{1+\alpha}}\right) + \left(-\frac{\partial p^{-}}{\partial x} + HaS\right)\mathrm{Sinh}\left(\frac{Ha\left(h_2-y\right)}{\sqrt{1+\alpha}}\right)\right)\right), \tag{3.12}$$

4 Propulsive velocity of swimming sheet

The flow rates of the self-propelled sperms taking place either above or below the swimming sheet are seen to be constant and which can be observed by integrating the continuity equation. Moreover, the pressure difference over the wavelength, Δp, is unchanged for both zones, thus, the volumetric flow rate across the channel Q can be given through the expression

$$Q^{-} = \int_{h_2}^{h_s} u^{-}(y)\mathrm{d}y, \quad Q^{+} = \int_{h_s}^{h_1} u^{+}(y)\mathrm{d}y, \tag{4.1}$$

Using Eqs. (3.11) and (3.12), Eq. (4.1) takes the forms

$$\Delta p = I_1 + I_2 Q^{+} + I_3 S + I_4 V_P, \qquad \Delta p = I_5 + I_6 Q^{-} + I_7 S + I_8 V_P, \tag{4.2}$$

where

$$I_1 = \int_0^1 F1Ha^3\left(h_1 - h_3\right)\mathrm{d}x, \quad I_2 = \int_0^1 Ha^3 F_1 \mathrm{d}x,$$

$$I_3 = \int_0^1 F_1\left(-Ha^2\left(h_1-h_3\right) + 2Ha\sqrt{1+\alpha}\,\mathrm{Tanh}\left(\frac{\left(h_1-h_3\right)Ha}{2\sqrt{1+\alpha}}\right)\right)\mathrm{d}x,$$

$$I_4 = \int_0^1 F_1\left(-Ha^3\left(h_1-h_3\right) + 2Ha^2\sqrt{1+\alpha}\,\mathrm{Tanh}\left(\frac{\left(h_1-h_3\right)Ha}{2\sqrt{1+\alpha}}\right)\right)\mathrm{d}x,$$

$$I_5 = \int_0^1 F_2 Ha^3\left(h_2 - h_3\right)\mathrm{d}x, \quad I_6 = \int_0^1 -Ha^3 F_2 \mathrm{d}x,$$

$$I_7 = \int_0^1 -F_2\left(Ha^2\left(h_2-h_3\right) - 2Ha\sqrt{1+\alpha}\,\mathrm{Tanh}\left(\frac{\left(h_2-h_3\right)Ha}{2\sqrt{1+\alpha}}\right)\right)\mathrm{d}x,$$

$$I_8 = \int_0^1 -F_2\left(Ha^3\left(h_2-h_3\right) - 2Ha^2\sqrt{1+\alpha}\,\mathrm{Tanh}\left(\frac{\left(h_2-h_3\right)Ha}{2\sqrt{1+\alpha}}\right)\right)\mathrm{d}x,$$

and

$$F_i = \frac{1}{\left(-h_i + h_3\right)Ha + 2\sqrt{1+\alpha}\,\mathrm{Tanh}\left(\frac{\left(h_i-h_3\right)Ha}{2\sqrt{1+\alpha}}\right)}.$$

Since the swimming sheet of spermatozoa is self-propulsive, the forces exerted by the fluid on it must balance for its motion to be of constant velocity V_P (Smelser et al. 1974). Mathematically, we can write this down as

$$\int_0^1 \left(\tau_{xy}{}^{+} - \tau_{xy}{}^{-} - b_s \sin 2\pi x\left(\frac{\partial p^{+}}{\partial x} - \frac{\partial p^{-}}{\partial x}\right)\right)\mathrm{d}x = 0, \tag{4.3}$$

i.e.

$$I_9 V_P + I_{10} Q^{+} + I_{11} Q^{-} + I_{12} = 0, \tag{4.4}$$

where

$$I_9 = \int_0^1 \left(K_1 - K_2 - \frac{G_1}{F_1} + \frac{G_2}{F_2} \right) \mathrm{d}x,$$

$$I_{10} = \int_0^1 F_1 Ha^2 \left(Habs\mathrm{Sin}(x) + 2\sqrt{1+\alpha}\,\mathrm{Tanh}\left(\frac{(h_1 - h_3)Ha}{2\sqrt{1+\alpha}} \right) \right) \mathrm{d}x,$$

$$I_{11} = \int_0^1 F_2 Ha^2 \left(Habs\mathrm{Sin}(x) + 2\sqrt{1+\alpha}\,\mathrm{Tanh}\left(\frac{(h_2 - h_3)Ha}{2\sqrt{1+\alpha}} \right) \right) \mathrm{d}x,$$

$$\begin{aligned} I_{12} = \int_0^1 & \left(F_1 Ha^2 (h_1 - h_3)\right. \\ & \left(bs\mathrm{Sin}(x) + 2\sqrt{1+\alpha}\,\mathrm{Tanh}\left(\frac{(h_1 - h_3)Ha}{2\sqrt{1+\alpha}} \right) \right) \\ & -F_2 Ha^2 (h_2 - h_3) \\ & \left.\left(bs\mathrm{Sin}(x) + 2\sqrt{1+\alpha}\,\mathrm{Tanh}\left(\frac{(h_2 - h_3)Ha}{2\sqrt{1+\alpha}} \right) \right)\right) \mathrm{d}x, \end{aligned}$$

$$K_i = Ha\sqrt{1+\alpha}\,\mathrm{Tanh}\left(\frac{(h_i - h_3)Ha}{2\sqrt{1+\alpha}} \right),$$

$$\begin{aligned} G_i = Ha\Bigg(& (h_i - h_3)Ha\sqrt{1+\alpha}\,\mathrm{Coth}\left(\frac{(h_i - h_3)Ha}{2\sqrt{1+\alpha}} \right) \\ & -(h_i - h_3)Ha\sqrt{1+\alpha}\,\mathrm{Csch}\left(\frac{(h_i - h_3)Ha}{2\sqrt{1+\alpha}} \right) \\ & +bs(h_i - h_3)Ha^2\mathrm{Sin}(x) \\ & -bsHa\sqrt{1+\alpha}\,\mathrm{Sin}(x)\mathrm{Tanh}\left(\frac{(h_i - h_3)Ha}{2\sqrt{1+\alpha}} \right) \\ & -(1+\alpha)\mathrm{Tanh}^2\left(\frac{(h_i - h_3)Ha}{2\sqrt{1+\alpha}} \right) \Bigg), \text{ and } i = 1, 2 \end{aligned} \tag{4.5}$$

By solving Eqs. (4.2) and (4.4), then the propulsive velocity V_P takes the form

$$V_P = \frac{-I_{11}I_2I_5 - I_{10}I_1I_6 + I_{12}I_2I_6 - (I_{10}I_3I_6 + I_{11}I_2I_7)s + (I_{11}I_2 + I_{10}I_6)\Delta P}{I_{10}I_4I_6 + I_{11}I_2I_8 - I_9I_2I_6}. \tag{4.6}$$

5 Results and discussion

The aim of this section is to investigate the impact of the pertinent parameters on the physical expressions involved in the flow model. Mathematica program has been used in order to study the physical influence of the Eyring–Powell fluid parameter $\boldsymbol{\alpha}$, electric field strength parameter $\boldsymbol{S}$, Hartmann number $\boldsymbol{Ha}$, wave amplitude on the cervical wall $\boldsymbol{b_w}$, and propulsive velocity $\boldsymbol{V_p}$ on the distributions of streamlines, mucus velocities of cervical canal $\boldsymbol{u}^{\pm}$, pressure gradients $\frac{\partial p^{\pm}}{\partial x}$, and pressure difference over wavelength $\Delta \boldsymbol{p}$. Since the problem involves upper and lower swimming sheets, in the ongoing discussion, the positive and negative superscripts denote the upper and lower swimming sheets, respectively, for the physical variable under consideration. Also, the blue and red colors in the graphs are meant to indicate the variations in the upper and lower sheets, respectively.

5.1 Streamlines of the electro-magnetic cervical flow

Figures 3, 4, 5, 6, 7, and 8 are made to observe the effects of the pertinent parameters on the streamlines' pattern of the lubricious cervical canal. For the sake of conciseness, one parameter is varied at a time while others are kept constant. Figures 3 and 4 represent the behavior of the circulating bolus for the swimmers above and below the micro-organism surface sheet under the effect of the magnetic parameter. It is noticed that there are circulating zones above and below the swimmer surface at a small value of Ha $(=1.5)$ after which they are reduced with an increase in Ha until void zones are observed with no trapped bolus. One possible reason for the reduction of trapped bolus is that the swimmers move faster before they reach simultaneity and extend in a form of sinusoidal shape along the channel. Figures 5 and 6 elucidate the behavior of streamlines with different values of the propulsive velocity for the upper and lower sheets. It is observed that the number of trapped zones is decreasing with an increase in V_p for both sheets. It is also noticed that the circulating bolus near to the walls disappears with an increase in V_p leaving bigger trapped region away from the boundary for both the upper and lower sheets. Figures 7 and 8 give an insight into the variations taking place in the trapped bolus under the effect of the fluid parameter α for the upper and lower sheets, respectively. It is noticed that the size of trapped bolus is increased in the corresponding middle regions in both halves of the canal for the non-Newtonian fluid $(\alpha = 2)$ than that of the Newtonian fluid $(\alpha = 0)$. It is also observed that the number of circulating zones remains unchanged.

5.2 Mucus velocities

Figure 9a–c displays the behavior of the mucus velocities that are plotted versus y above and below the swimming sheet for various values of the pertinent parameters. It is seen from Fig. 9a that the mucus velocity profile

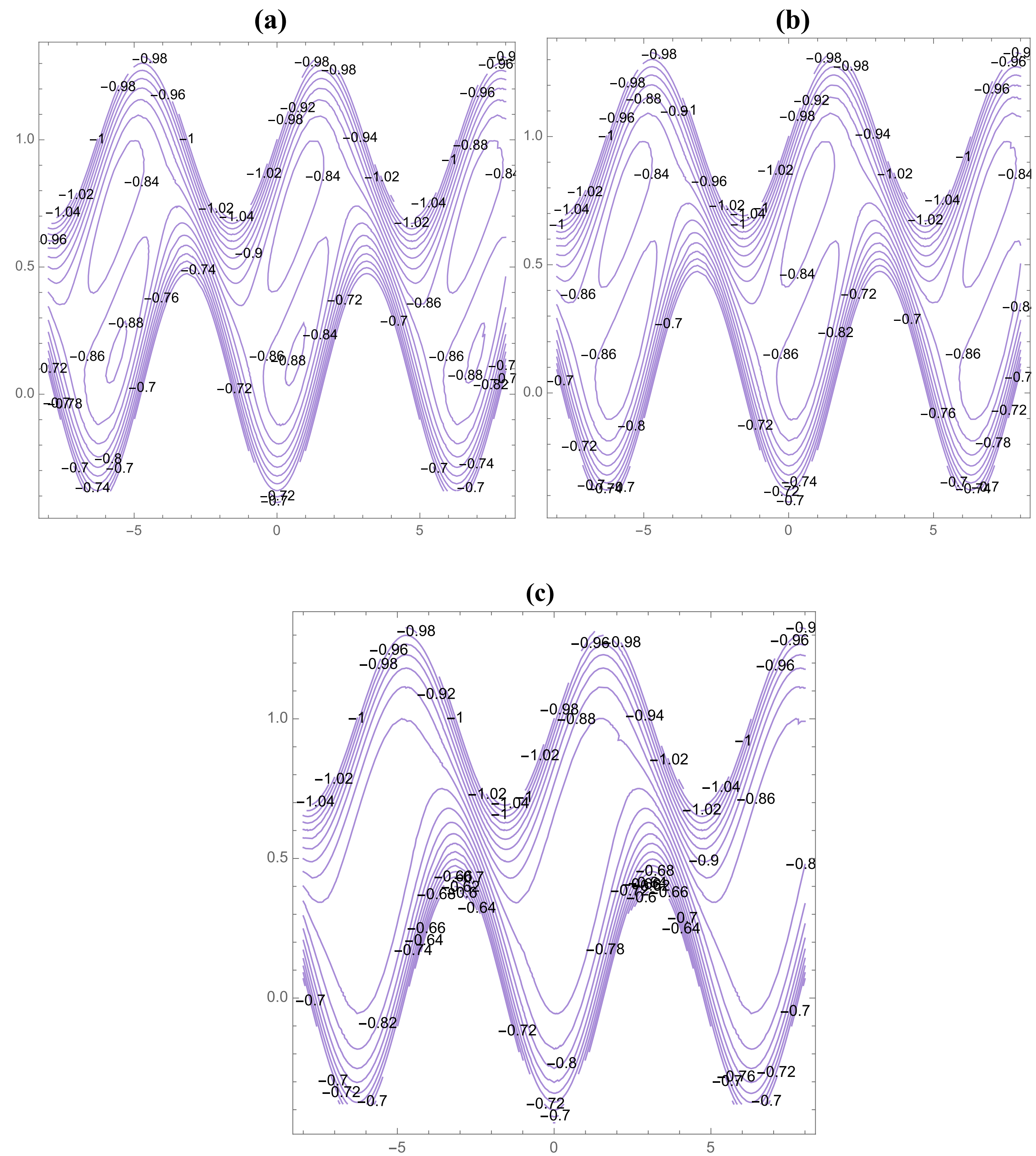

Fig. 3 Streamlines of flow above the swimming sheet for Ha = 1.5 (**a**), Ha = 2 (**b**), and Ha = 5 (**c**) with V_p = 0.1, b_w= 0.35, b_s = 0.45, Q=−0.323, $\phi = \pi/2$,α = 0.1, and S=0.1

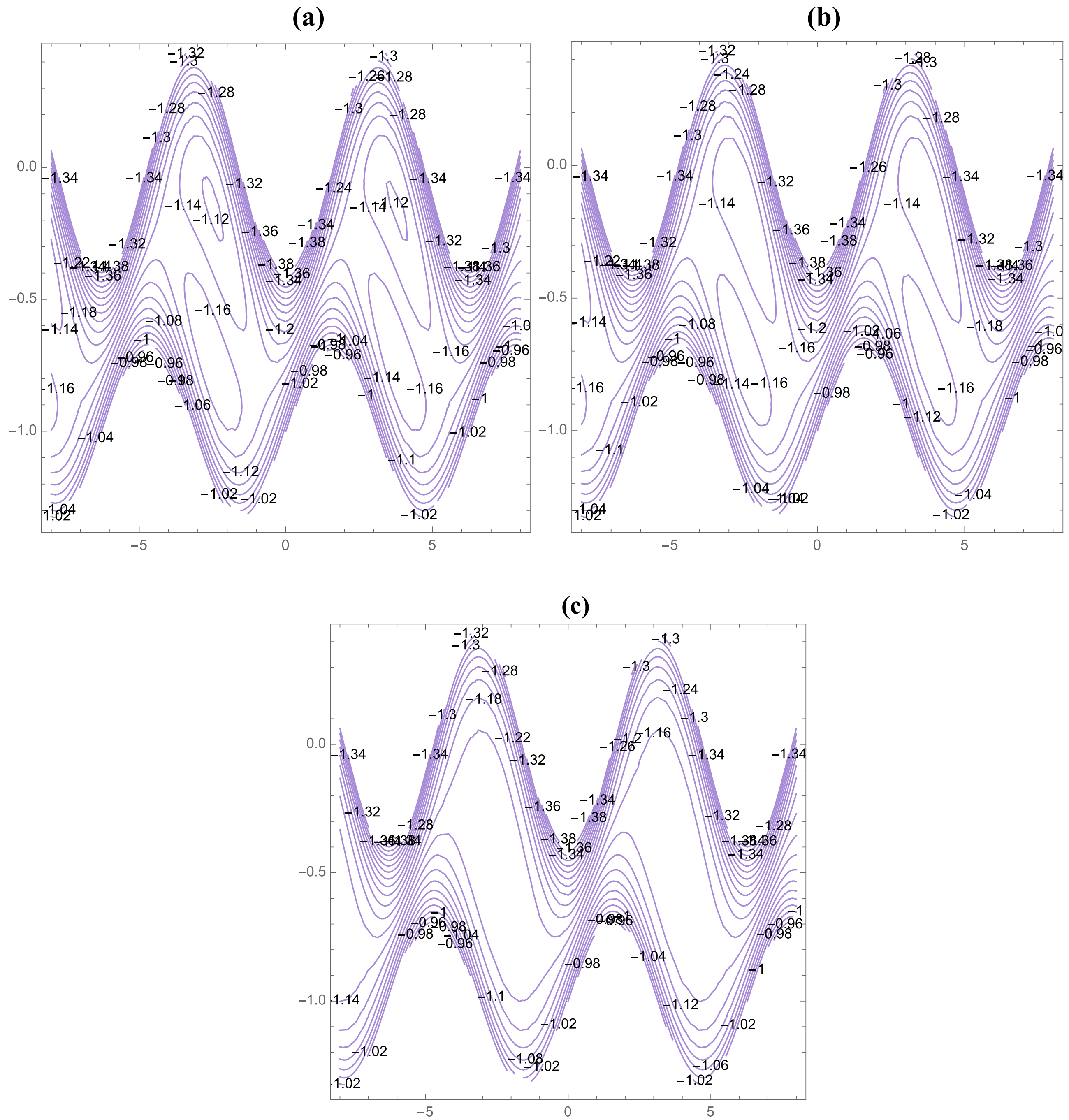

Fig. 4 Streamlines of flow below the swimming sheet for Ha = 1.5 (**a**), Ha = 2 (**b**), and Ha = 5 (**c**) with V_p = 0.1, b_w= 0.35, b_s = 0.45, Q=−0.323, $\phi = \pi/2$,α = 0.1, and S=0.2

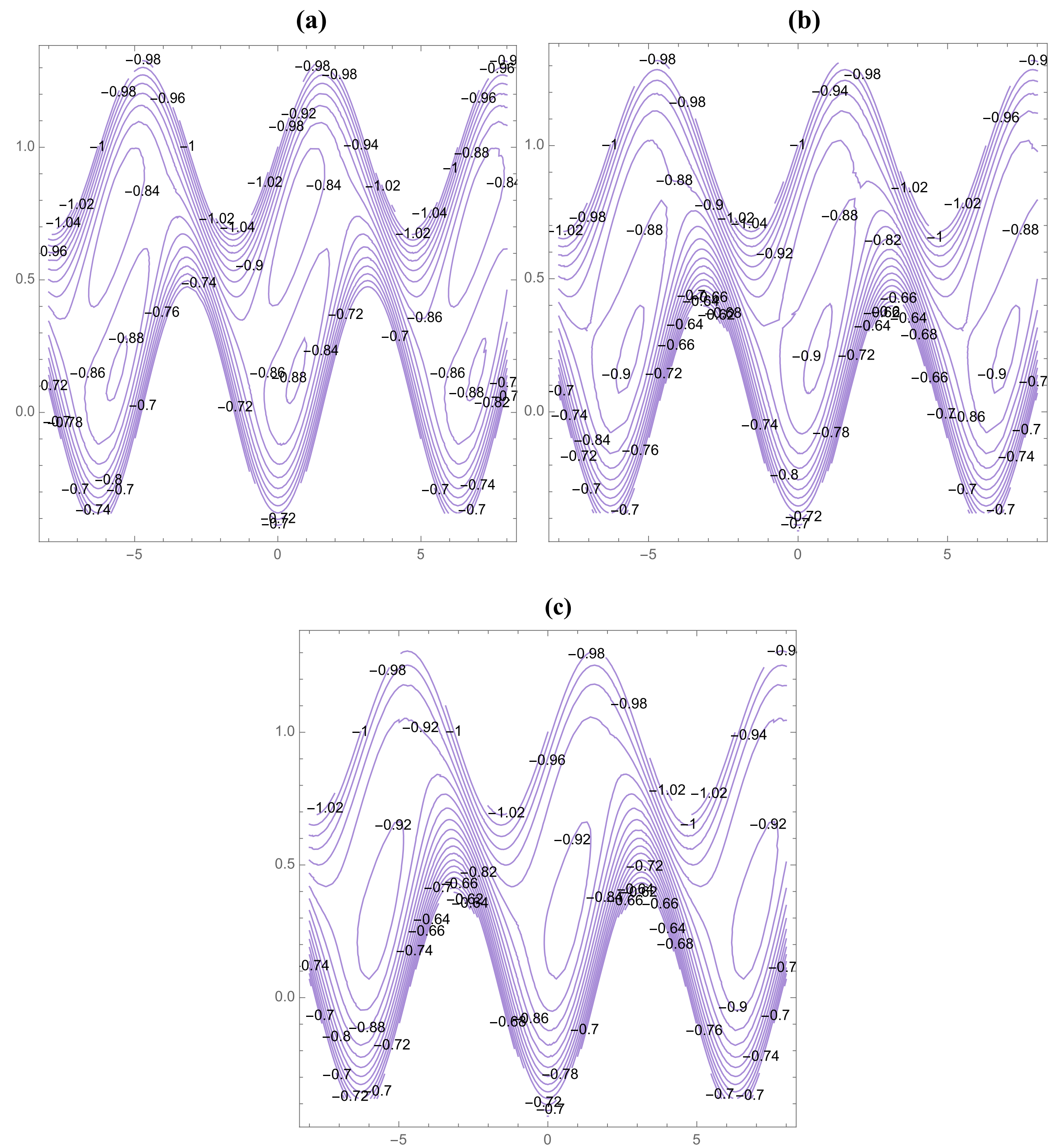

Fig. 5 Streamlines of flow above the swimming sheet for $V_p = 0.1$ (**a**), $V_p = 0.3$ (**b**), and $V_p = 0.5$ (**c**) with $Ha = 1.5$, $b_w = 0.35$, $b_s = 0.45$, $Q = -0.323$, $\phi = \pi/2, \alpha = 0.1$, and $S = 0.1$

increases with an increase in α below the swimming sheet while the behavior is totally reversed above the swimming sheet. Figure 9b depicts the variation of $u^{\pm}$ with y for various values of the magnetic parameter Ha. It is seen that the mucus velocity profile increases with an increase in Ha below the swimming sheet, and it continues increasing slightly until it reaches $y = 0.25$. Figure 9c exhibits the effect of S on the mucus velocities where it is observed that they increase with an increase in S above and below the swimming sheet. It is generally

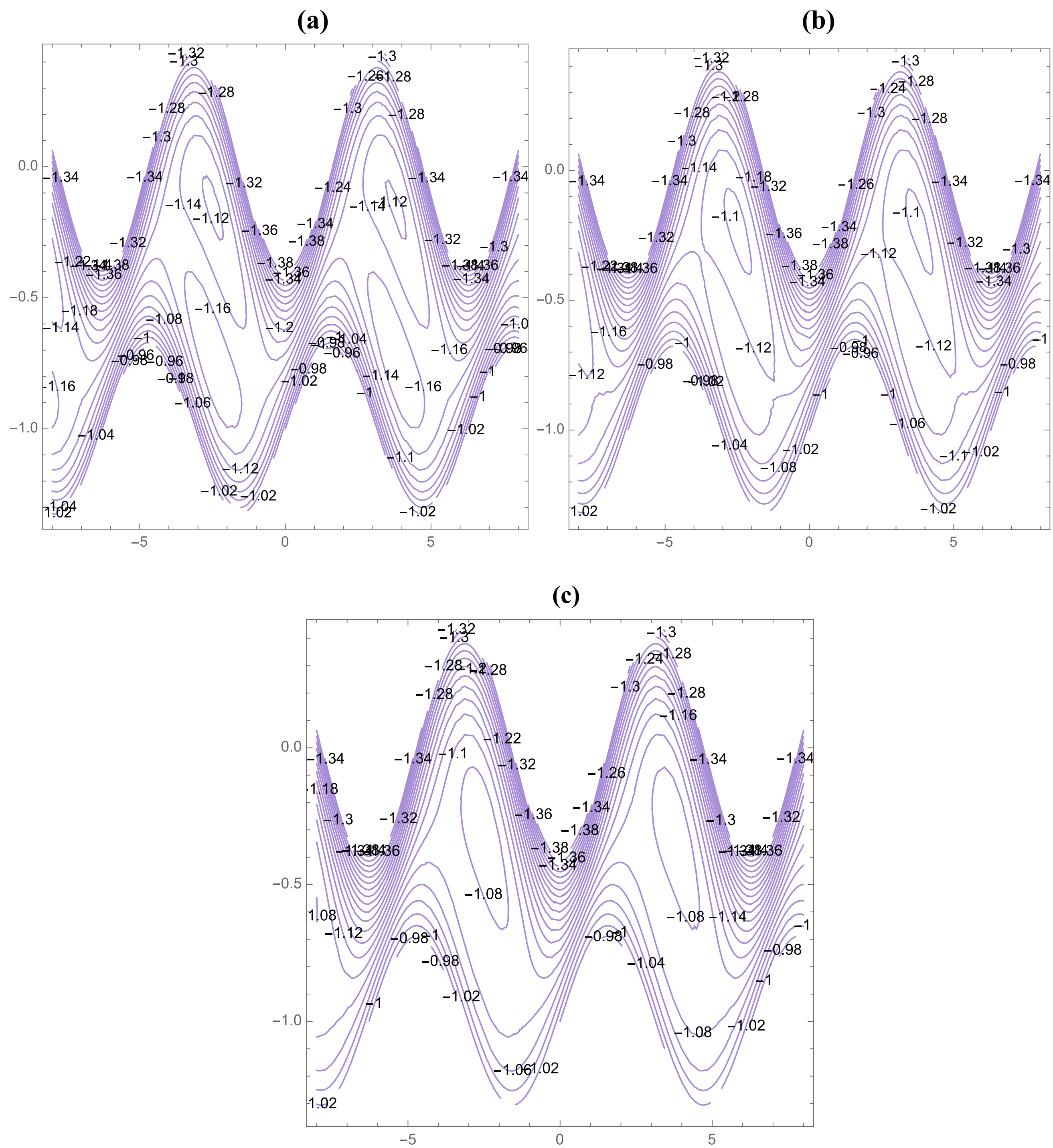

Fig. 6 Streamlines of flow below the swimming sheet for $V_p = 0.1$ (**a**), $V_p = 0.3$ (**b**), and $V_p = 0.5$ (**c**) with $Ha = 1.5$, $b_w = 0.35$, $b_s = 0.45$, $Q = -0.323$, $\phi = \pi/2$, $\alpha = 0.1$, and $S = 0.1$

observed that the velocity profiles of cervical mucus are not parabolic (not a Poiseuille flow). Further, it is seen that the mucus velocities at the walls h_1 and h_2 are not equal which validates the boundary conditions. It is also observed that mucus velocity attains least values in the absence of electric field.

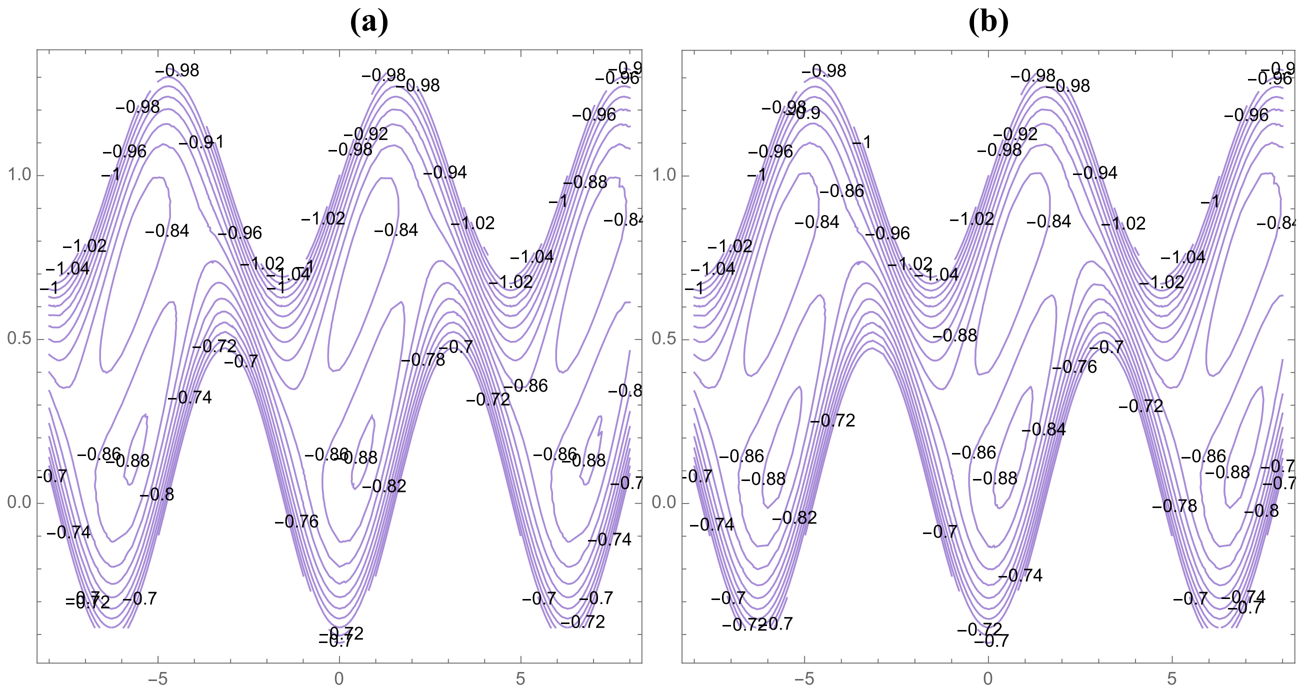

Fig. 7 Streamlines of flow above the swimming sheet for $\alpha = 0$ (**a**) and $\alpha = 2$ (**b**) with $Ha = 1.5$, $b_w = 0.35$, $b_s = 0.45$, $Q = -0.323$, $\phi = \pi/2$, $V_p = 0.1$, and $S = 0.1$

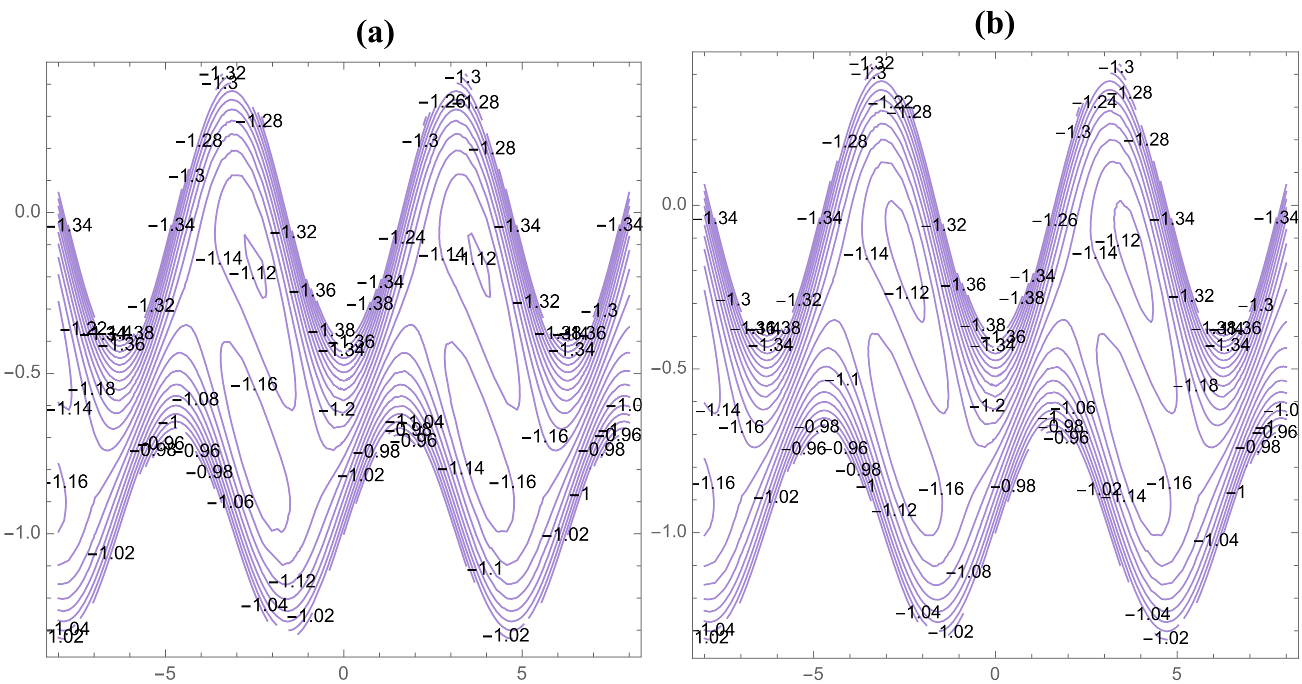

Fig. 8 Streamlines of flow below the swimming sheet for $\alpha = 0$ (**a**) and $\alpha = 2$ (**b**) with $Ha = 1.5$, $b_w = 0.35$, $b_s = 0.45$, $Q = -0.323$, $\phi = \pi/2$, $V_p = 0.1$, and $S = 0.2$

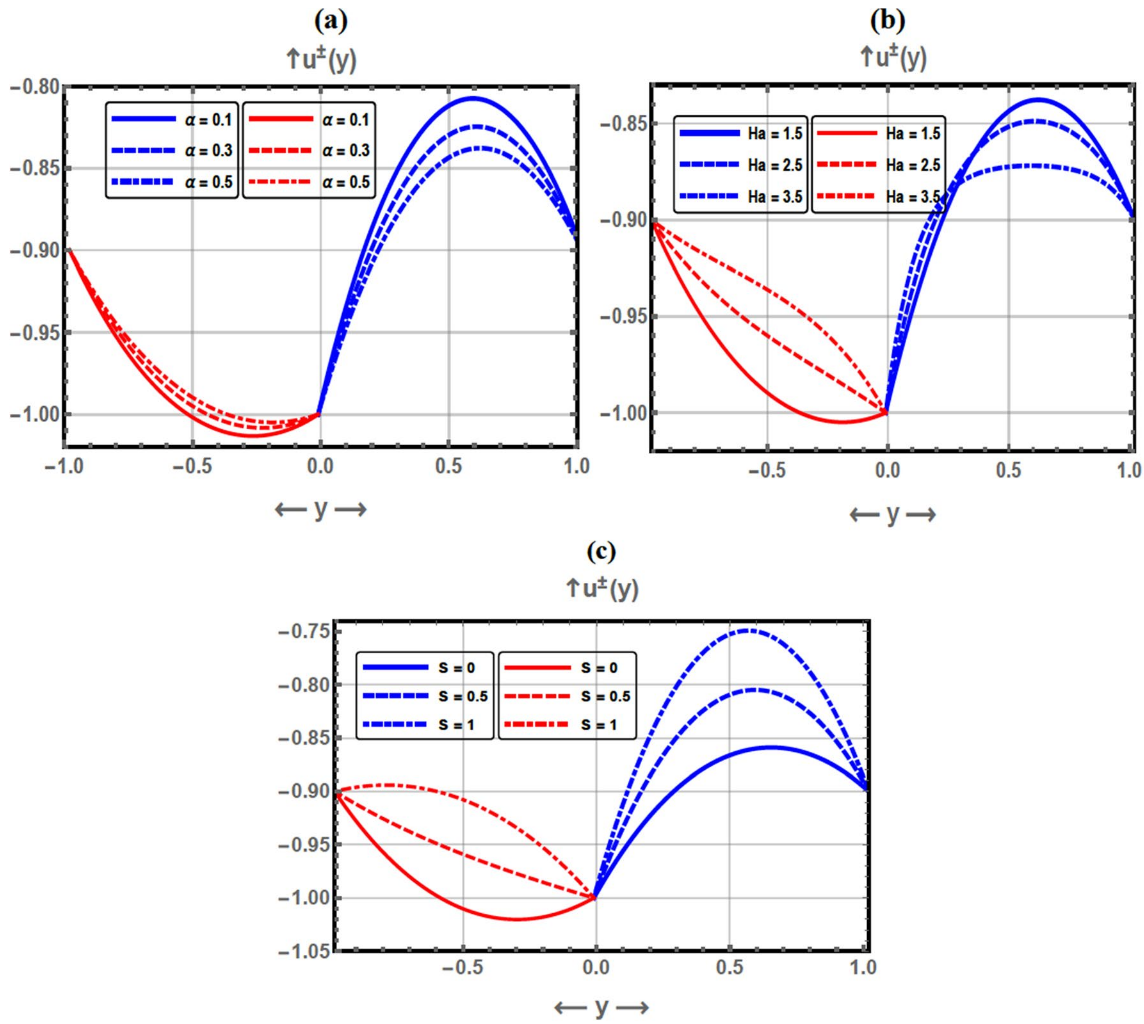

Fig. 9 Plots for mucus velocities below and above the swimming sheet: for various values of α with $V_p = 0.1$, $b_w = 0.1$, $b_s = 0.01$, $\phi = \pi/2$, $Ha = 1.5$, $S{=}0.2$, $Q{=}{-}0.1$, and $x{=}0.2$ (**a**); Ha with $V_p = 0.1$, $b_w = 0.1$, $b_s = 0.01$, $\phi = \pi/2$, $\alpha = 0.5$, $S{=}0.2$, $Q{=}{-}0.1$, and $x{=}0.2$ (**b**); and S with $V_p = 0.1$, $b_w = 0.1$, $b_s = 0.01$, $\phi = \pi/2$, $\alpha = 0.5$, $Ha = 1.5$, $Q{=}{-}0.1$, and $x{=}0.2$ (**c**)

5.3 Pressure gradients

Figure 10a–e is plotted in order to investigate the dependency of the pressure gradients above and below the swimming sheet upon Ha, S, α, b_w, and V_p. Figure 10a reveals that the pressure gradient increases noticeably with an increase in the magnetic parameter above and below the swimming sheet. Similarly, it can be inferred from Fig. 10b, e that the electric field and propulsive velocity enhance the pressure gradient substantially above and below the swimming sheet. Moreover, it is observed that $\frac{\partial p^{\pm}}{\partial x}$ attains least values in the absence of electric field. It is also seen from Fig. 10e that the pressure gradient is minimum in the absence of propulsive velocity. Figure 10c describes the behavior of $\frac{\partial p^{\pm}}{\partial x}$ with α from which we conclude that an increase in α causes an increase in the pressure gradient below the swimming sheet until a specific value of y $(=3.6)$ before the effect is reversed with an obvious incremental decrease along the y-axis. Alternatively, it is also shown that above the swimming sheet, α has an incremental effect on $\frac{\partial p^{\pm}}{\partial x}$ where it is seen to diminish slowly until $y{=}2.6$ before it starts to increase progressively afterwards with α. Further, it is observed that $\frac{\partial p^{\pm}}{\partial x}$ attains least values for Newtonian fluid than that of non-Newtonian fluid. It is observed from Fig. 10d that unlike the behavior of $\frac{\partial p^{\pm}}{\partial x}$ with b_w above the swimming sheet, $\frac{\partial p^{\pm}}{\partial x}$ is seen to increase below the swimming sheet until $y{=}3.2$ before it starts to increase with an increase in b_w. It is generally noticed that the amplitude of pressure gradient increases above the swimming sheet with gradual changes in the parameters of interest.

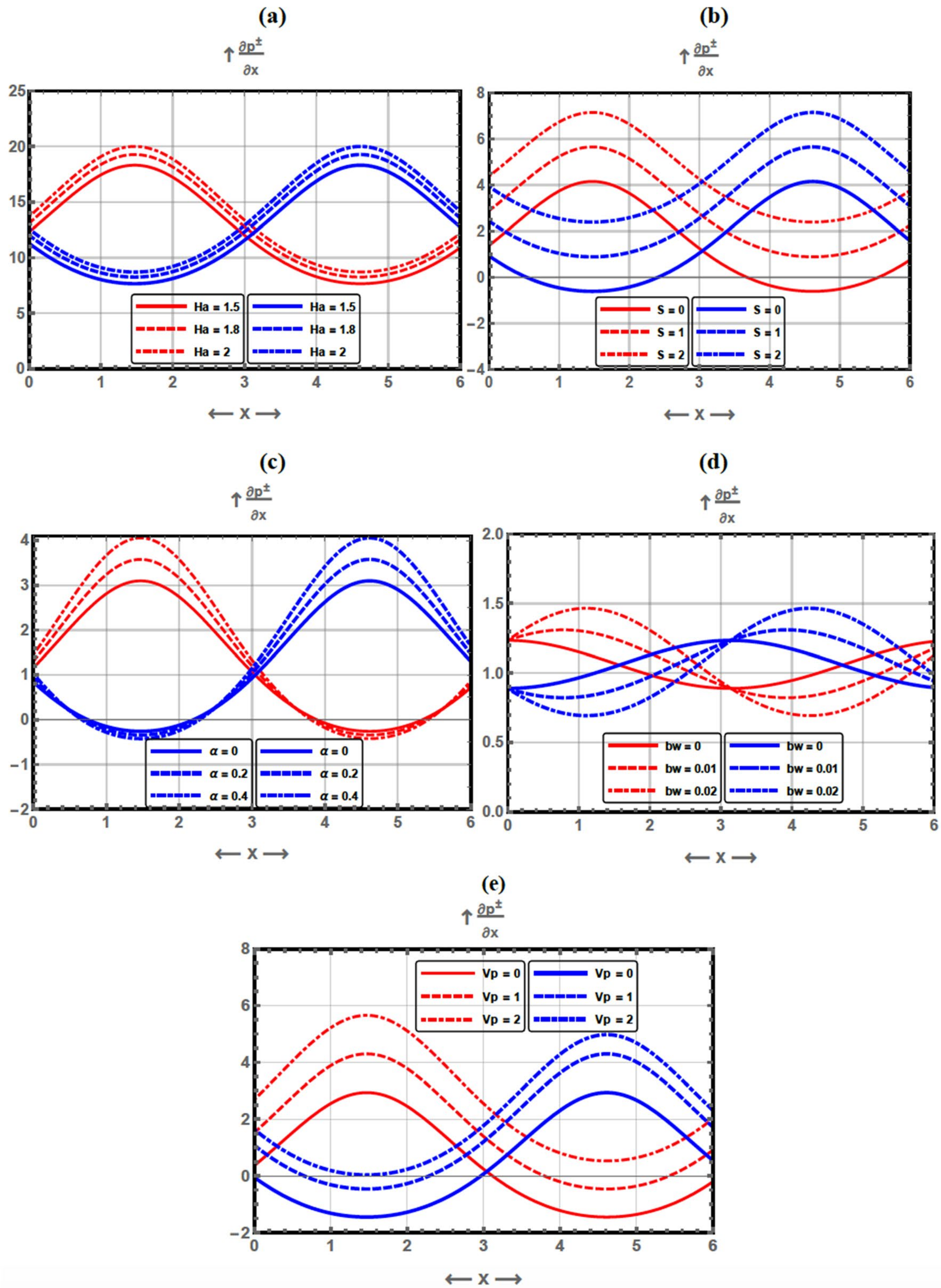

Fig. 10 Plots for pressure gradients below and above the swimming sheet: for various values of Ha with $V_p = 0.1$, $b_w = 0.1$, $b_s = 0.01$, $\phi = \pi/2$, $\alpha = 0.5$, $S = 0.2$, $Q = -1.5$, and $y = 0.1$ (**a**); S with $V_p = 0.1$, $b_w = 0.1$, $b_s = 0.01$, $\phi = \pi/2$, $\alpha = 0.5$, $Ha = 1.5$, $Q = -1$, and $y = 0.1$ (**b**); α with $S = 0.1$, $b_w = 0.1$, $b_s = 0.01$, $\phi = \pi/2$, $V_p = 0.1$, $Ha = 1.5$, $Q = -1$, and $y = 0.1$ (**c**); b_w with $S = 0.1$, $\alpha = 0.1$, $b_s = 0.01$, $\phi = \pi/2$, $V_p = 0.1$, $Ha = 1.5$, $Q = -1$, and $y = 0.1$ (**d**); and V_p with $S = 0.1$, $b_w = 0.1$, $b_s = 0.01$, $\phi = \pi/2$, $\alpha = 0.5$, $Ha = 1.5$, $Q = -1$, and $y = 0.1$ (**e**)

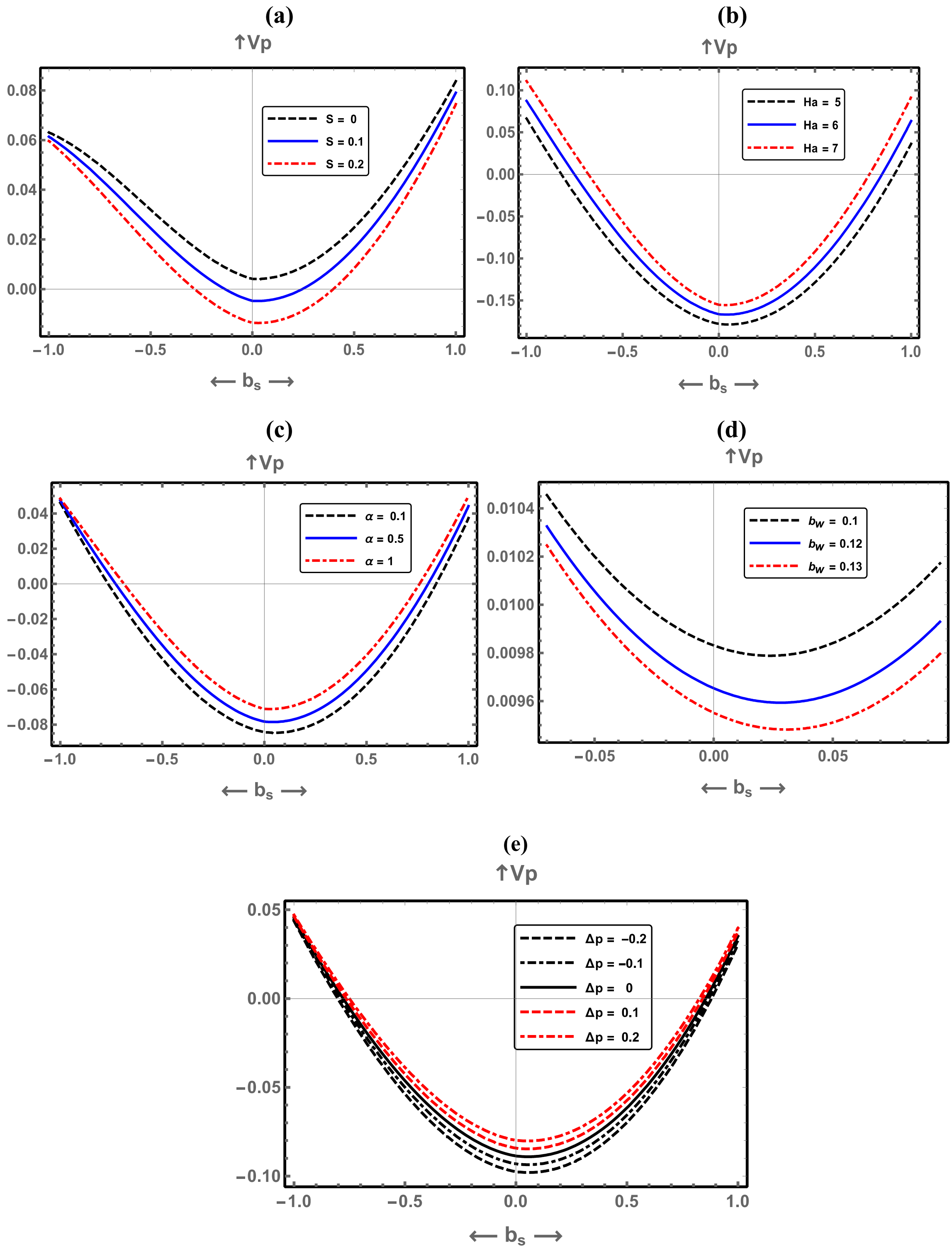

Fig. 11 Plots for propulsive velocity: for various values of S with b_w= 0.1, $\phi = \pi$, $\alpha = 0.1$, $\Delta p = 0.1$, and $Ha=2$ (**a**); Ha with b_w= 0.1, $\phi = \pi$, $\alpha = 0.1$, $\Delta p = 0.1$, and $S=2$ (**b**); α with b_w= 0.1, $\phi = \pi$, $Ha=2$, Δp = 0.1, $Ha=2$, and $S=1$ (**c**); b_w with=Δp0.2, $\phi = \pi$, $Ha=2$, $S=1$, and $\alpha = 0.1$ (**d**); and b_w= 0.1, $\phi = \pi$, $Ha=2$, s=1, and $\alpha = 0.1$ (**e**)

5.4 Propulsive velocity

The propulsive velocity of the swimming sheet V_p depends upon the electric field S, Hartmann number Ha, Eyring–Powell fluid parameter α, wave amplitude on the cervical wall b_w, and pressure difference over wavelength Δp. Figure 11a–e are plotted in order to observe the effects of the pertinent parameters on V_p. It is noticed that Ha and α have an increasing effect on V_p as seen in Fig. 11b, c. A quite opposite behavior is noticed from V_p with an increase in S and b_w as seen in Fig. 11a, d. That is, it is concluded that in order to minimize the speed of spermatozoa, it is best to apply an electric field on the flow. This means that applying electric field on the flow is very important in controlling the transport of spermatozoa inside the cervical canal. Figure 11e discloses the behavior of the propulsive velocity with Δp where an enhancement in V_p with an increase in Δp is shown. Hence, the pressure difference over wavelength boosts the velocity of sperms and assists the sperms' movement to fertilize the ovum in the female's reproductive system when Δp attains zero or positive values, whereas the pressure drop is seen to inhibit the chances of pregnancy by thrusting the sperms from the uterus to the vagina. The latter result conforms with that obtained by Walait et al. (2018) for a flow through slippery cervical canal.

5.5 Pumping characteristics

We recall that the swimming sperms have propulsive velocity V_p taking place from the vagina to the uterus in a negative

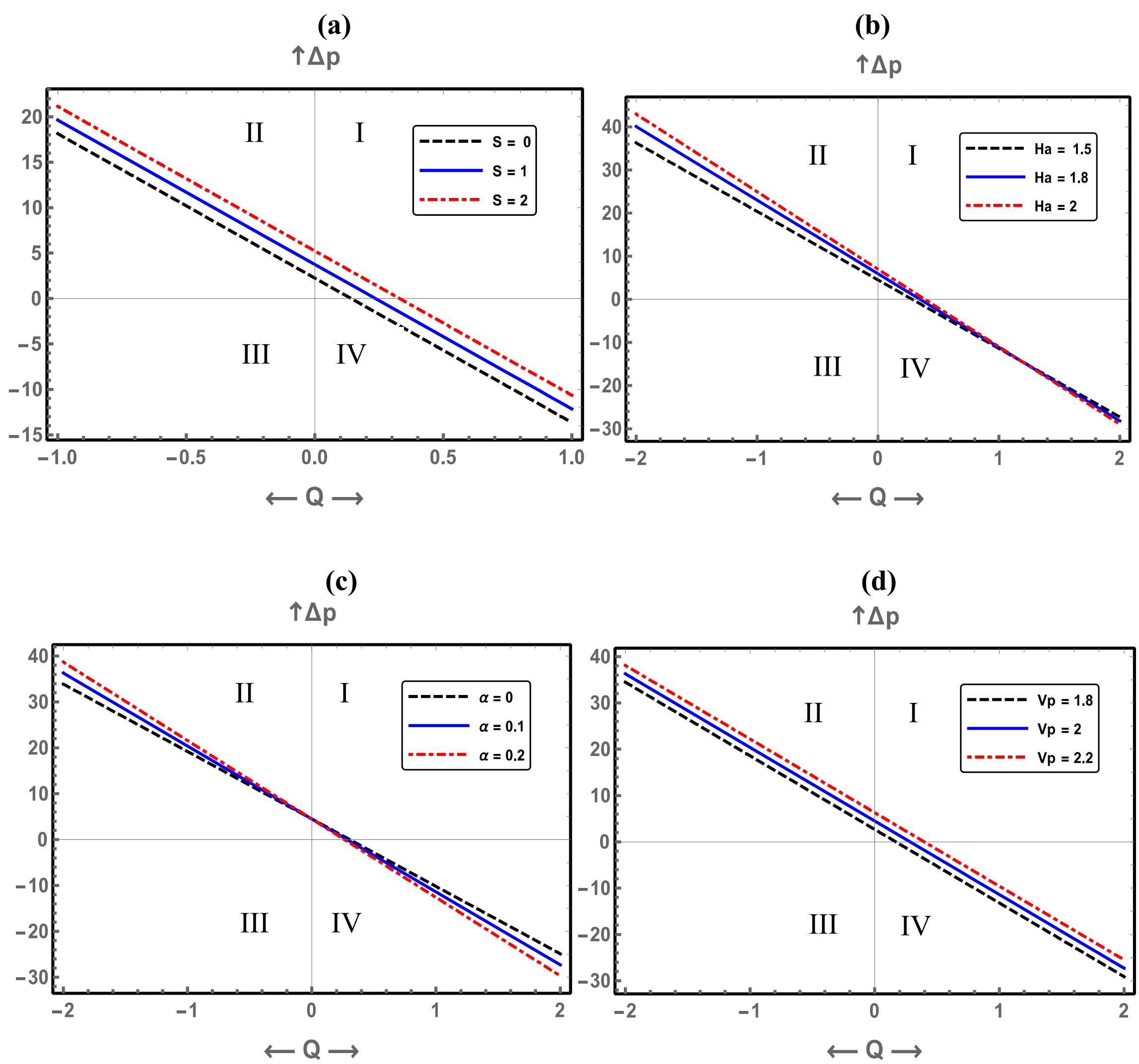

Fig. 12 Plots for pressure rise versus mean flow rate: for various values of S with $b_w = 0.1$, $\phi = \pi$, $\alpha = 0.1$, $b_s = 0.1$, $\Delta p = 0.1$, $Ha = 1.5$, and $V_p = 2$; Ha with $b_w = 0.1$, $\phi = \pi$, $\alpha = 0.1$, $b_s = 0.1$, $S = 1.5$, and $V_p = 2$; α with $b_w = 0.1$, $\phi = \pi$, $b_s = 0.1$, $S = 1.5$, and $V_p = 2$; and V_p with $b_w = 0.1$, $\phi = \pi$, $b_s = 0.1$, $S = 1.5$, $Ha = 1.5$, and $\alpha = 0.1$

x-direction whereas the traveling waves on the canal walls propagate along the positive x-axis from the uterus to the vagina. Figure 12a–d elucidates the pumping characteristics of the swimming sheet of sperms along the main direction of the flow, i.e. from the vagina to the uterus. We investigate the dependence of the pressure difference over wavelength Δp, which is the same above and below the swimming sheet as aforementioned, upon S, Ha, α, and V_p. And in doing so, one must characterize the regions of pumping mechanism. The pressure difference over wavelength is sectored into four major quadrants. The first quadrant ($P > 0$ and $Q > 0$) that represents the cervical sinusoidal pumping region through which the flow rate is totally due to the traveling waves on the cervical wall after overcoming the self-propulsion of sperms and pressure difference. The second quadrant ($P > 0$ and $Q < 0$) that represents the retrograde pumping region through which the flow takes place in the direction of the swimming sheet of sperms. The third quadrant ($P < 0$ and $Q < 0$) that represents the self-propulsion pumping region through which the self-propulsive waves dominates the traveling waves and the pressure difference assists the flow that takes place from the vagina to the uterus. And finally, the fourth quadrant ($P < 0$ and $Q < 0$) that represents the augmented pumping region through which the pressure difference amplifies the flow. Figure 12a investigates the dependence of Δp upon S where it is noticed that the pumping rate increases with an increase in S in the cervical sinusoidal, retrograde, and augmented pumping regions. Further, it is seen that Δp attains the least values in the absence of electric field. A similar behavior is seen for Δp with V_p as shown in Fig. 12d. It is depicted from Fig. 12b that the pumping rate is enhanced by an increase in Ha in the retrograde and cervical sinusoidal pumping regions, while it is reduced incrementally in the augmented pumping region. Figure 12c illustrates that the pumping rate increases with an increase in α in the retrograde pumping region, then the effect of α is seen to be minimal in the cervical sinusoidal region before the pumping rate is noticed to be reduced in the augmented pumping region. Unlike the behavior of Δp in the augmented region, it is observed that it is smaller for Newtonian fluid than that of non-Newtonian fluid in the retrograde pumping region. Generally, it is also observed that there is no flow in the self-propulsion region due to the bigger amplitude of traveling waves in comparison to the self-propulsive wave especially with the existence of S that reduces the propulsive velocity as aforementioned in the previous section.

6 Concluding remarks

In this work, biomechanics of the swimming of sperms through cervical canal is investigated through electrically-conducting biofluid with an external magnetic field being applied on the flow in transverse direction. Eyring–Powell model is considered as the base fluid to simulate male's semen with self-propulsive sperms. The governing partial differential equations are analytically solved, and long wavelength approximation is employed. The distributions of velocity, stream function, pressure gradient, and pressure gradient were calculated and presented with various of the pertinent parameters. The proposed model can be applied in controlling swimming sperms through 2D conduits that account for females' cervical canals filled with mucus. The main observations can be concluded as follows:

i. There is a critical value for Hartmann number after which the circulating zones are reduced above and below the swimmer surface.
ii. The size of trapped bolus is increased throughout the canal for the non-Newtonian fluid than that of the Newtonian fluid.
iii. The mucus velocities increase with an increase in the electric field above and below the swimming sheet.
iv. The pressure gradient is minimum in the absence of propulsive velocity.
v. The electric field and propulsive velocity enhance the pressure gradient substantially above and below the swimming sheet.
vi. Unlike the behavior of the propulsive velocity with the electric field, it seems to be increasing with an increase in Hartmann number, Eyring–Powell parameter, and the wave amplitude on the cervical wall.
vii. The mucus velocity and the pressure gradient attain the least values throughout the flow in the absence of electric field.
viii. The pressure gradient below and above the swimming sheet attains the least values for Newtonian fluid than that of non-Newtonian fluid.
ix. The pressure difference accelerates the motion of sperms in order to fertilize the ovum in the female's reproductive tract.
x. The pressure drop inhibits the chances of pregnancy by thrusting the sperms from the uterus to the vagina.
xi. The electric field reduces the pressure difference substantially.
xii. Unlike the behavior of pressure difference in the augmented region, it is observed that it is smaller for Newtonian fluid than that of non-Newtonian fluid in the retrograde pumping region.
xiii. Solving our problem for Newtonian fluid in the absence of electric field implies to a well-agreed physical situation as obtained by Asghar et al. (2019) for Newtonian fluid.
xiv. Solving our model for Newtonian fluid and in the absence of electric and magnetic fields, our investiga-

tion is in good agreement with that obtained by Walait et al. (2018) for non-slip flow.

xv. Investigating our problem for Newtonian fluid in the absence of magnetic and electric fields, our model reduces to that of Smelser et al. (1974)

Acknowledgements This work has been accomplished under a bilateral cooperation agreement between TWAS-UNESCO and Universidad Nacional Autónoma de México in Juriquilla, Querétaro. Sara I. Abdelsalam would like to acknowledge TWAS-Italy for the financial support of her visit to UNAM under the TWAS-UNESCO Associateship. The author also thanks the FORDECYT-CONACYT for the financial support under the aforementioned agreement. Special thanks are given to Professor Marcelo Aguilar, the Instituto de Matemáticas of UNAM, for facilitating the visit.

Author contributions S.I. Abdelsalam conceived the presented idea and the basic framework. A.Z. Zaher developed the theory, carried out the computations and produced the graphs. S.I. Abdelsalam verified the analytical methods and solutions. A.Z. Zaher wrote the modeling section and the solutions. S.I. Abdelsalam wrote the abstract, introduction, discussion, conclusion, and reference sections. J.X. Velasco-Hernández revised the manuscript. S.I. Abdelsalam supervised the findings of this work.

Compliance with ethical standards

Competing interests The authors declare that they have no conflict of interest.

References

Abd Elmaboud Y, Abdelsalam SI, Mekheimer KhS, Vafai K (2019) Electromagnetic flow for two-layer immiscible fluids. Eng Sci Technol Int J 22(1):237–248

Abdelsalam SI, Bhatti MM (2018) The impact of impinging TiO_2 nanoparticles in Prandtl nanofluid along with endoscopic and variable magnetic field effects on peristaltic blood flow. Multidiscip Model Mater Struct 14(3):530–548

Abdelsalam SI, Sohai M (2020) Numerical approach of variable thermophysical features of dissipated viscous nanofluid comprising gyrotactic micro-organisms. Pramana J Phys 94:67–79

Abdelsalam SI, Vafai K (2017) Combined effects of magnetic field and rheological properties on the peristaltic flow of a compressible fluid in a microfluidic channel. Eur J Mech B Fluids 65:398–411

Abo-Elkhair RE, Mekheimer KhS, Zaher AZ (2018) Electro-magnetohydrodynamic oscillatory flow of a dielectric fluid through a porous medium with heat transfer: Brinkman model. BioNanoScience. https://doi.org/10.1007/s12668-018-0515-6

Asghar Z, Ali N, Sajid M, Anwar Bég O (2019) Magnetic microswimmers propelling through biorheological liquid bounded within an active channel. J Magn Magn Mater. https://doi.org/10.1016/j.jmmm.2019.165283

Bhatti MM, Zeeshan A, Ijaz N, Anwar Bég O, Kadir A (2017) Mathematical modelling of nonlinear thermal radiation effects on EMHD peristaltic pumping of viscoelastic dusty fluid through a porous medium duct. Eng Sci Technol Int J. https://doi.org/10.1016/j.jestch.2016.11.003

Bhatti MM, Riaz A, Zhang L, Sadiq MS, Ellahi R (2020) Biologically inspired thermal transport on the rheology of Williamson hydromagnetic nanofluid flow with convection: an entropy analysis. J Therm Anal Calorim. https://doi.org/10.1007/s10973-020-09876-5

Buren M, Jian Y (2015) Electromagnetohydrodynamic (EMHD) flow between two transversely wavy micro parallel plates. Electrophoresis 36:1539–1548

Carlson BM (2019) The human body, chapter 14—the reproductive system. Andre Gerhard Wolff, London, pp 373–396

Davajan V, Nakamura RM, Kharma K (1970) Spermatozoan transport in cervical mucus. Obsrer Gynrc Survey 25:1–43

Dharmendra T, Prakash J, Tiwari AK, Ellahi R (2020) Thermal, microrotation, electromagnetic field and nanoparticle shape effects on Cu-CuO/blood flow in microvascular vessels. Microvasc Res 132:104065

Durairajanayagam D (2018) Lifestyle causes of male infertility. Arab J Urol 16:10–20

Eldesoky IM, Abdelsalam SI, El-Askary WA, Ahmed MM (2019) Concurrent development of thermal energy with magnetic field on a particle-fluid suspension through a porous conduit. BioNanoScience 9(1):186–202

Ellahi R, Shivanian E, Abbasbandy S, Hayat T (2016) Numerical study of magnetohydrodynamics generalized Couette flow of Eyring–Powell fluid with heat transfer and slip condition. Int J Numer Methods Heat Fluid Flow 26(5):1433–1445

Ellahi R, Sait SM, Shehzad N, Ayaz Z (2020) A hybrid investigation on numerical and analytical solutions of electro-magnetohydrodynamics flow of nanofluid through porous media with entropy generation. Int J Numer Methods Heat Fluid Flow 30:834–854

Ishaq M, Ali G, Shah SIA, Shah Z, Muhammad S, Hussain SA (2019) Nanofluid film flow of eyring powell fluid with magneto hydrodynamic effect on unsteady porous stretching sheet. J Math 51(2):131–153

Jones RE, Lopez KH (2014) Human reproductive biology (Fourth edition), Chapter 15—infertility, Elsevier, pp 283–299 (2014)

Kay VJ, de Silva SM (2020) Obesity, chapter 12—male obesity—impact on semen quality, Stacy Masucci, pp 119–126

Keramati H, Sadeghi A, Saidi MH, Chakraborty S (2016) Analytical solutions for thermo-fluidic transport in electroosmotic flow through rough micro-tubes. Int J Heat Mass Transf 92:244–251

Khan NA, Sohail A, Sultan F (2017) Effect of anisotropic slip and magnetic field on the flow and heat transfer of Eyring–Powell fluid over an infinite rotating disk. Int J Fluid Mech Res 44(3):257–273

Mekheimer KS, Elkomy SR, Abdelsalam SI (2013) Simultaneous effects of magnetic field and space porosity on compressible Maxwell fluid transport induced by a surface acoustic wave in a microchannel. Chin Phys B 22(12), 124702–1–10

Mekheimer KhS, Hasona WM, El-Shekhipy AA, Zaher AZ (2017) Electrokinetics of dielectric non-Newtonian bio fluids with heat transfer through a flexible channel: numerical study. Comput Methods Sci Technol 23:331–341

Morris L, Do V, Chard J, Brand AH (2017) Radiation-induced vaginal stenosis: current perspectives. Int J Women's Health 9:273–279

Nakano FY, Leão RDBF, Esteves SC (2015) Insights into the role of cervical mucus and vaginal pH in unexplained infertility. Med Express (São Paulo, online) 2(2). http://dx.doi.org/https://doi.org/10.5935/MedicalExpress.2015.02.07

Naz R, Shah Z, Kumam P, Thounthong P (2019) Exploration of temperature dependent thermophysical characteristics of yield exhibiting non-Newtonian fluid flow under gyrotactic microorganisms. AIP Adv 9:125016

Odeblad E (1962) Undulation of macromolecules in cervical mucus. Int J Fertil 7:313–319

Oyelami FH, Dada MS (2016) Transient magnetohydrodynamic flow of Eyring–Powell fluid in a porous medium. IFE J Sci 18(2):463–472
Pak OS, Lauga E (2010) The transient swimming of a waving sheet. Proc R Soc 466:107–126
Philip D, Chandra P (1995) Self-propulsion of spermatozoa in microcontinua: effect of transverse wave motion of channel walls. Arch Appl Mech 66:90–99
Radhakrishnamacharya G, Sharma R (2007) Motion of a self-propelling micro-organism in a channel under peristalsis: effects of viscosity variation. Nonlinear Anal Model Control 12:409–418
Reynolds AJ (1965) The swimming of minute organisms. J Fluid Mech 23:241–260
Shack WJ, Lardner TJ (1974) A long wavelength solution for a microorganism swimming in a channel. Bull Math Biol 36:435–444
Shafik A, El Sibai O, Shafik AA, Ahmed I, Mostafa RM (2004) The electrovaginogram: study of the vaginal electric activity and its role in the sexual act and disorders. Arch Gynecol Obstet 269:282–286
Shukla JB, Rao BRP, Parihar RS (1978) Swimming of spermatozoa in cervix: effect of dynamical interaction and peripheral layer viscosity. J Biomech 11:15–19
Shukla JB, Chandra P, Sharma R, Radhakrishnamacharya G (1988) Effects of peristaltic and longitudinal wave motion of the channel wall on movement of micro-organisms: application to spermatozoa transport. J Biomech 21:947–954
Sinha P, Singh C, Prasat KR (1982) A microcontinuum analysis of the self-propulsion of the spermatozoa in the cervical canal. Int J Eng Sci 20:1037–1048
Smelser RE, Shack WJ, Lardner TJ (1974) The swimming spermatozoa in an active channel. J Biomech 7:349–355
Sohail M, Ali U, Al-Mdallal Q, Thounthong P, Sherif E-SM, Alrabaiah H, Abdelmalek Z (2020a) Theoretical and numerical investigation of entropy for the variable thermophysical characteristics of couple stress material: applications to optimization. Alex Eng J. https://doi.org/10.1016/j.aej.2020.07.042
Sohail M, Naz R, Abdelsalam SI (2020b) On the onset of entropy generation for a nanofluid with thermal radiation and gyrotactic microorganisms through 3D flows. Phys Scr 95(4):045206
Sohail M, Naz R, Raza R (2020c) Application of double diffusion theories to Maxwell nanofluid under the appliance of thermal radiation and gyrotactic microorganism. Multidiscip Model Mater Struct 16:256–280
Sohail M, Shah Z, Tassaddiq A, Kumam P, Roy P (2020d) Entropy generation in MHD Casson fluid flow with variable heat conductance and thermal conductivity over non-linear bi-directional stretching surface. Sci Rep 10:1–16
Taylor GI (1951) Analysis of the swimming of microscopic organisms. Proc R Soc 209:447–461
Tuck EO (1968) A note on a swimming problem. J Fluid Mech 31:305–308
Walait A, Siddiqui AM, Rana MA (2018) Biomechanics of the swimming of self-propelling spermatozoa through slippery human cervical canal. Acta Mech 229:2861–2881
Zeeshan A, Shehzad N, Abbas T, Ellahi R (2019) Effects of radiative electro-magnetohydrodynamics diminishing internal energy of pressure-driven flow of titanium dioxide-water nanofluid due to entropy generation. Entropy 21(236):1–25
Zhang L, Bhatti MM, Michaelides EE (2020) Entropy Generation in magnetized blood flow through a finite wavy channel under slip conditions. J Non-Equilib Thermodyn 45:419–429